# A Mueller-Matrix Formalism for Modeling Polarization Azimuth and Ellipticity Angle in Semiconductor Optical Amplifiers in a Pump–Probe Scheme

L. Q. Guo and Michael J. Connelly, *Member, IEEE*

***Abstract*—This paper presents a Mueller-matrix approach to simulate the azimuth and ellipticity trajectory of a probe light in a tensile-strained bulk semiconductor optical amplifier (SOA) in a conventional pump–probe scheme. The physical mechanisms for the variations of polarization azimuth and ellipticity angle of the probe originate from the significant nonuniform distributions of carrier density across the active region in the presence of an intense pump light. Due to this carrier-density nonuniformity, the effective refractive indexes experienced by transverse-electric (TE) and transverse-magnetic (TM) modes of the probe are different. This results in a phase shift between TE and TM modes of the probe upon leaving the SOA. Simulations of the carrier distributions along the cavity length at different pump-light levels are demonstrated using multisection rate equations, which take into account the longitudinal nonuniform carrier density. The optical gain is considered via the parabolic band approximation. The influences of the spontaneous recombination and carrier-dependent material loss on the amplifier performance are included. The Mueller-matrix formalism is utilized to predict the variations of azimuth and ellipticity angle, which greatly reduces the complexity of the simulations in comparison with Jones-matrix formalism. The suggested approach is beneficial to experimental investigations due to the fact that during the optical-tuning process, Stokes parameters are virtually measurable on the Poincaré sphere, and the Stokes vector of the incoming probe can be adjusted by a polarization controller and monitored by a polarization analyzer. Based on these carrier-induced nonlinearities in SOAs, an optical AND gate with extinction ratio larger than 14 dB and Q-factor larger than 25 is presented at a bit rate of 2.5 Gb/s.**

***Index Terms*—Azimuth, ellipticity, modeling, Mueller matrix, semiconductor optical amplifier (SOA), Stokes parameters.**

## I. Introduction

THERE HAS been considerable recent progress in the exploitation of optical nonlinearities in semiconductor optical amplifiers (SOAs) [1]–[3]. Much attention has been paid to the carrier-induced nonlinearities, which lead to nonlinear polarization rotation in SOAs either in the co- or counter-propagation scheme. The main reason for the effort is that: This nonlinear phenomenon is a mixture of cross-phase and cross-gain-modulation (XGM) effects in an SOA causing nonlinear polarization rotation of a probe in the presence of an intense pump light [4] and shows great potential of applications in optical networks [5]–[8]. Several models have been published to simulate the carrier-induced nonlinearities in SOAs. Alvarez *et al.* [9] demonstrated the confinement-factor difference between transverse-electric (TE) and transverse-magnetic (TM) mode on the dependence of the carrier density in a bulk SOA, whereas Zhao *et al.* [10] predicted the polarization variations of the probe light as a function of its power level and the bias current of SOAs, but no pump light was involved in their model. Soto *et al.* [11] investigated the phase-shift efficiency in terms of pump- and probe-light polarization in a pump–probe scheme, and Dorren *et al.* [6] extended the theory and applied it to all-optical flip-flop memories. To the best of our knowledge, no model has yet utilized Mueller matrix and Stokes vectors to investigate the nonlinear polarization rotation, which is caused by the carrier-induced nonlinearities in SOAs. Compared with Jones-matrix approach, the superiority of Mueller-matrix formalism lies in its simplicity and easy measurement in the form of Stokes parameters. In this paper, we report theoretical and experimental investigations of nonlinear polarization rotation in a tensile-strained bulk SOA, which answers the question we raised in [5]. The phase "nonlinear polarization rotation" is used throughout this paper in the sense of the changes of polarization azimuth and/or ellipticity angle.

This paper gives results from a detailed multisection-rate-equation model to approximate the carrier-induced nonlinearities in SOAs with a manageable parabolic function of the carrier density, which contributes to the refractive-index difference between TE and TM mode of a probe light. The variations of Stokes vectors are treated by Mueller-matrix formalism, and the polarization azimuth and ellipticity angle are predicted. Experimental measurements of the ellipticity-angle variations are performed, showing good agreement with the model predictions and validating the impacts of nonuniform carrier density on TE/TM refractive index.

This paper is organized as follows: In Section II, a detailed multisection-rate-equation model is presented, focusing on the nonuniform distributions of carrier density as a function of pump-light levels. The refractive-index difference between TE

Manuscript received December 14, 2006; revised August 2, 2006. This work was supported by the Science Foundation Ireland under Investigator Grant 02/IN1/I42.

The authors are with Optical Communications Research Group, Department of Electronic and Computer Engineering, University of Limerick, 2 Limerick, Ireland (e-mail: li-qiang.guo@ul.ie).

Color versions of one or more of the figures in this paper are available online at http://ieeexplore.ieee.org.

Digital Object Identifier 10.1109/JLT.2006.886674

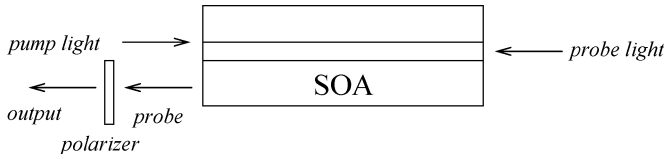


Fig. 1. Schematic diagram of a pump–probe scheme employing an SOA as nonlinear medium. Counter propagation is demonstrated and the ellipticity variation of the probe is detected by a polarizer.

and TM mode, which results from this nonuniform carrier density, is estimated, and the variations of azimuth and ellipticity of the probe are treated by the Mueller-matrix formalism.

In Section III, the simulation results are demonstrated in comparison with experimental investigations. The comparison highlights the simplicity and efficiency of using the Mueller matrix, instead of the Jones matrix, when modeling the polarization variations of a probe light in pump and probe geometry.

As an important application of this nonlinear effect, optical AND gate is demonstrated in Section IV, showing high Q-factor and large extinction ratio. Some interesting points related to the system performance are made in Section V, and conclusions reached in this paper are summarized in Section VI.

## II. Theory

A conventional pump–probe scheme employing an SOA as nonlinear medium is depicted in Fig. 1. Counter propagation is used, and the ellipticity variation of the probe is detected by a polarizer at the output of the SOA. One of the great strengths of the pump–probe technique is that it can be used, with essentially no change in the experimental setup, to measure pump-induced refractive-index nonlinearities [12].

The nonlinear polarization rotation of a probe light in SOAs is caused by different refractive index of TE and TM mode, and this difference is due to intrinsic birefringence [13] and optically induced birefringence in SOAs [5]. The induced birefringence is closely related to nonuniform carrier density in the amplifier cavity. Therefore, we first solve the rate equation of the SOA, compute the carrier density, and determine the refractive index for TE and TM mode. With the help of the Mueller-matrix approach, we simulate the azimuth and ellipticity angle of the probe.

### A. Rate-Equation Model

The intricate relationships between carrier density, light intensity, and SOA physical parameters are usually described by a rate equation. At any axial point in the cavity, the rate at which carriers recombine must be balanced with the injection current and pump-light intensity. The steady-state rate equation used in the model is given in (1), which is based on the standard equations used by, e.g., [14] and [15], with the inclusion of a few details to account for SOA active region of bulk material in the presence of spontaneous emission

$$\frac{dn}{dt} = \frac{\eta \cdot J}{q \cdot d} - \frac{n}{\tau} - \frac{g \cdot I_{\mathrm{av}}}{E} - g_{\mathrm{mp}} \cdot S_{\mathrm{sp}} \tag{1}$$

where

| | |
|---|---|
| $n$ | carrier density; |
| $J$ | current density; |
| $d$ | active-layer thickness; |
| $q$ | electronic charge; |
| $\tau$ | carrier recombination lifetime; |
| $g$ | optical gain coefficient; |
| $E$ | photon energy; |
| $g_{\mathrm{mp}}$ | material-gain coefficient at peak wavelength. |

In (1), $\eta$ is the current-injection efficiency due to the possible existence of leakage currents. $I_{\mathrm{av}}$ represents the average intensity of the input light along the cavity length. $S_{\mathrm{sp}}$ is the photon density due to the amplified spontaneous emission (ASE).

The gain spectrum is assumed to be parabolic, and the material gain, which depends on the carrier density in the active region, can be approximated by [14]

$$g_m = a_1(n - n_0) - a_2(\lambda - \lambda_p)^2 \tag{2}$$

where $a_1$ and $a_2$ are the material-gain constants. $\lambda_p$ is the peak gain wavelength and depends on carrier density $n$ [14]

$$\lambda_p(n) = \lambda_0 - a_3(n - n_p) \tag{3}$$

where $\lambda_0$ and $n_p$ are the peak gain wavelength and the carrier density at the original threshold of the amplifier, respectively. $a_3$ is a material-gain constant. Therefore, the carrier-density-dependent optical gain can be expressed by

$$g = \Gamma g_m - \alpha \tag{4}$$

where $\Gamma$ is the optical confinement factor, and $\alpha$ is the material-loss coefficient.

Instead of treating it as a constant, the material-loss coefficient $\alpha$ is modeled as a linear function of carrier density [16], taking into account of longitudinal nonuniformity, as expected from the relationship

$$\alpha(n) = \alpha_1 + \alpha_2 n \tag{5}$$

where $\alpha_1$ is the loss coefficient due to the transitions between the split-off band and the acceptor level, which is almost constant for carrier density $n$ [17], and $\alpha_2$ is the loss coefficient due to the transitions between the split-off and heavy-hole valence band and is the constant proportionality connecting the carrier density $n$ with $\alpha$.

The average light intensity $I_{\mathrm{av}}$ can be estimated by [18]

$$I_{\mathrm{av}} = I_{\mathrm{input}} \frac{G_s - 1}{gL} \tag{6}$$

where $L$ is the cavity length, and $G_s$ is the single-pass gain, which is given by

$$G_s = \exp\left[(\Gamma g_m - \alpha) \cdot L\right]. \tag{7}$$

It has been reported that the bimolecular and Auger recombination are important phenomena in InGaAsP/InP material system [19]. To include their influences on the performance of

the amplifier, a detailed recombination model is used, in which both are included

$$\tau = \frac{1}{A + Bn + Cn^2} \tag{8}$$

where $A$ is the so-called Schockley–Read–Hall (or leakage) coefficient, and $B$ is the bimolecular-radiative-rate coefficient that for high carrier densities, becomes carrier-density-dependent. Experimentally, it has been shown that

$$B(n) = B_0 - B_1 n \tag{9}$$

where $B_0$ and $B_1$ are coefficients determined by the pump–probe measurements [19], [20]. However, an accurate mathematical description of this carrier-density-dependent coefficient is an involved task that is beyond the scope of this paper. Therefore, for the ease of analysis, $B$ is assumed constant. $C$ is the Auger-recombination coefficient due to many different forms of Auger-recombination process [21]. In this paper, we simply take $C$ as a constant to represent the main nonradiative recombination process in SOAs [23]

$$S_{\rm sp} = \frac{\beta \cdot R(n)}{2(\Gamma g_m - \alpha)} \cdot \left[ \frac{(R_1+R_2)(G_s-1)^2 + 2(1-R_1R_2G_s)(G_s-1)}{L(\Gamma g_m - \alpha)(1-R_1R_2G_s^2)} - 2 \right]. \tag{10}$$

The amplified spontaneous photon density $S_{\rm sp}$, averaged over the amplifier cavity length, is given in (10), where $R(n)$ is the spontaneous emission rate assuming bimolecular recombination $Bn^2$, $R_1$ and $R_2$ are facet reflectivity of the amplifier, and $\beta$ is the spontaneous emission factor. We acknowledge that $\beta$ is not a constant [22], since the spontaneous emission is not uniformly distributed among the various cavity modes. In a more detailed analysis, $\beta$ can be written as the product of a geometric spontaneous emission factor $\beta_g$ and a spectral spontaneous emission factor $\beta_s$ [24]. $\beta_g$ gives the probability that a spontaneously emitted photon is captured by the mode of interest, whereas $\beta_s$ is a function of the parameters that describe the material properties of the active region and gives the fraction of the spontaneous emission that has the mode energy and polarization. However, it is beyond the scope of this paper to go into a detailed discussion of this topic and for the sake of brevity of simulation, in the rate-equation analysis, $\beta$ is approximated as a constant. This is justified for traveling-wave (TW)-type SOAs or SOAs with very low facet reflectivities.

### B. Multisection Steady-State Solutions

In the SOA active region, the carrier density and photon density are not uniform along the amplifier cavity length since the photon number increases strongly within the amplifier while the carrier density decreases owing to stimulated emission [25]. Meanwhile the optical gain and spontaneous emission rate are all functions of position in the amplifier. For TW amplifiers or amplifiers with very low facet reflectivities, the nonuniformity of the carrier density and photon density along the cavity length has to be considered. A sectioning approach is used to solve (1), taking into account the longitudinal variations of the carrier density. The amplifier is, therefore, divided into a number of longitudinal sections, which are considered as having a uniform carrier density

$$\frac{dn_i}{dt} = \frac{\eta \cdot J}{q \cdot d} - \frac{n_i}{\tau_i} - \frac{g_i \cdot I_{{\rm av}i}}{E} - g_{\rm mp} \cdot S_{{\rm sp}i} \tag{11}$$

where index $i$ refers to different amplifier sections.

Thus, each section in the SOA can now be treated as an individual TW-type SOA cavity and the rate equations are solved numerically to find the steady-state characteristics for a given pump-power level. The carrier density $n_i$ can be obtained in each section from numerical solutions of (2)–(8), and (10), and the outputs of each section are just the inputs of next section. The pump power is increased by small increments and a Newton–Ralphson method is used iteratively to find the carrier and photon densities at each value of the pump power. This approach is valid as long as the starting point of the pump power is not less than $-10$ dBm and the increments are kept small.

### C. Phase Shift of the Probe Light in a Pump–Probe Scheme

In pump and probe geometry, when an intense pump light is coupled into the SOA, the effective refractive indexes for TE and TM propagation along the semiconductor waveguide are given by [4]

$$N_{\rm TE} = N_{\rm TE0} + \Gamma_{\rm TE} \cdot n \cdot \left( \frac{dN_{\rm TE}}{dn} \right) \tag{12}$$

$$N_{\rm TM} = N_{\rm TM0} + \Gamma_{\rm TM} \cdot n \cdot \left( \frac{dN_{\rm TM}}{dn} \right) \tag{13}$$

where $N_0$ is the effective refractive index of the waveguide for zero carrier density, and $(dN/dn)$ is the rate of change of the active-layer refractive index with the carrier density $n$ (differential refractive index). $N_0$ is different for TE/TM mode, owing to the TE/TM asymmetry in semiconductor waveguide [13]. In our previous work [5], we have demonstrated that this pump-induced TE/TM index nonlinearity leads to a significant relative phase shift between TE and TM propagation of the probe light traveling inside the SOA, which can be expressed as

$$\Delta\varphi = k \cdot L \cdot (N_{\rm TE} - N_{\rm TM}) \tag{14}$$

where $k = 2\pi/\lambda_{\rm probe}$ is the propagation constant of the probe light in a vacuum.

As stated in Section II-B, because of carrier depletion due to stimulated emission, the carrier density along the SOA waveguide is not uniform ($n$ is a function of position $z$ along the cavity length). Therefore, $N_{\rm TE}$ and $N_{\rm TM}$ in (12) and (13), respectively, not only depend on the carrier density in the amplifier cavity but also the position of interest along the cavity

length. The local effective refractive indexes for TE and TM mode vary linearly with $n(z)$ as

$$N_{\mathrm{TE}}(z) = N_{\mathrm{TE0}} + \Gamma_{\mathrm{TE}} \cdot n(z) \cdot \left(\frac{dN_{\mathrm{TE}}}{dn}\right) \tag{15}$$

$$N_{\mathrm{TM}}(z) = N_{\mathrm{TM0}} + \Gamma_{\mathrm{TM}} \cdot n(z) \cdot \left(\frac{dN_{\mathrm{TM}}}{dn}\right). \tag{16}$$

Therefore, the overall phase shift should be a summation of local phase shift in each individual section in the amplifier. Following the multisection solutions for carrier density $n(z)$, which we discussed in (11), the total phase shift of the probe light upon leaving the SOA can be obtained by the following integration over the cavity length of the amplifier:

$$\Delta\varphi = k \int_0^L [N_{\mathrm{TE}}(z) - N_{\mathrm{TM}}(z)]\, dz. \tag{17}$$

Quite clearly, $\Delta\varphi$ is closely related to the longitudinal carrier density $n(z)$, which is a result of multisection solutions solved by (2)–(8), (10), and (11). In what follows, we will define the polarization-azimuth and ellipticity-angle variations with the carrier density in the SOA cavity.

### D. Mueller Matrix

The state of polarization (SOP) of the output light from the SOA is generally elliptical (a linear polarization can be seen as a special case of the elliptical polarization). It can be described by a Stokes vector. Azimuth, ellipticity, amplitude, and absolute phases are all closely related to Stokes parameters. The representation of the SOP of a fully polarized light on the Poincaré sphere is displayed in Fig. 2. As we previously demonstrated in [26], in a pump–probe scheme, the optical-tuning process can be virtually guided by a moving polarization trace on the Poincaré sphere and Stokes parameters are given simultaneously, which can be used for numerical simulations.

Given the Stokes parameters $S$ ($S_0$, $S_1$, $S_2$, and $S_3$) of the incoming probe light and $S'$ ($S'_0$, $S'_1$, $S'_2$, and $S'_3$) of the transmitted probe light upon leaving the SOA, the two Stokes vectors are related by the Mueller matrix

$$S' = M \cdot S \tag{18}$$

where $M$ is the Mueller matrix of the SOA.

Physically, the SOA can be treated as a polarization element, which alters the polarization state of the probe by changing the amplitude and the phase of its electric-field vector. Since optical gain and loss in SOAs are different for TE/TM propagation, the amplitudes of the electric-field vector of TE/TM mode of the probe are changed by different amounts. In this sense, the SOA works as a diattenuator. Meanwhile, the TE/TM mode of the probe experience different refractive index, as discussed in Section II-C, which results in different phase shift upon leaving the SOA. In this sense, the SOA behaves as a phase shifter. In a simplified but physically useful picture, the SOA can be treated simultaneously as a diattenuator and a phase shifter and its optical behavior can be described by a Mueller matrix given in (19), shown at the bottom of the page, which is originally constructed for an anisotropic absorbing retarder [27]. $G_{\mathrm{TE/TM}}$ is a single-pass gain for TE/TM propagation, and $\Delta\varphi$ is the total phase shift given in (17).

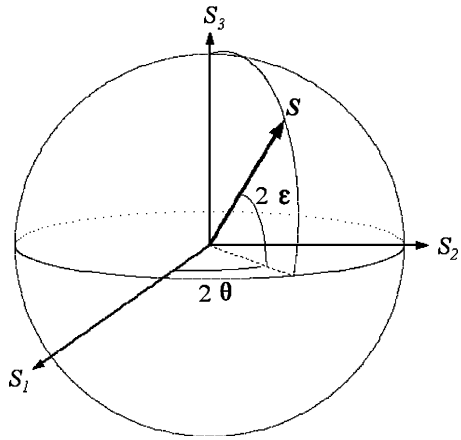


Fig. 2. Poincaré sphere representation of the SOP of a fully polarized light. $\theta$: polarization azimuth. $\varepsilon$: ellipticity angle.

In a polarization-insensitive SOA, optical gain for TE and TM mode are identical, $G_{\mathrm{TE}} = G_{\mathrm{TM}}$ can be assumed within the SOA gain bandwidth. Therefore, the calculations of the polarization azimuth $\theta$ and the ellipticity angle $\epsilon$ of the transmitted probe light can be greatly simplified. They can be expressed in terms of the Stokes parameters $S$ ($S_0$, $S_1$, $S_2$, and $S_3$) of the incoming probe light, and the phase shift $\Delta\varphi$ caused by the pump light in the SOA

$$\tan 2\theta = \frac{S_2 \cdot \cos\Delta\varphi + S_3 \cdot \sin\Delta\varphi}{S_1} \tag{20}$$

$$\sin 2\varepsilon = \frac{-S_2 \cdot \sin\Delta\varphi + S_3 \cdot \cos\Delta\varphi}{S_0}. \tag{21}$$

So far, given the Stokes parameters of the incoming probe light and the Mueller matrix of the SOA, the polarization azimuth and ellipticity angle of the probe upon leaving the SOA can be simulated.

$$M = \frac{1}{2}\begin{pmatrix} G_{\mathrm{TE}}^2 + G_{\mathrm{TM}}^2 & G_{\mathrm{TE}}^2 - G_{\mathrm{TM}}^2 & 0 & 0 \\ G_{\mathrm{TE}}^2 - G_{\mathrm{TM}}^2 & G_{\mathrm{TE}}^2 + G_{\mathrm{TM}}^2 & 0 & 0 \\ 0 & 0 & 2G_{\mathrm{TE}}G_{\mathrm{TM}}\cos\Delta\varphi & 2G_{\mathrm{TE}}G_{\mathrm{TM}}\sin\Delta\varphi \\ 0 & 0 & -2G_{\mathrm{TE}}G_{\mathrm{TM}}\sin\Delta\varphi & 2G_{\mathrm{TE}}G_{\mathrm{TM}}\cos\Delta\varphi \end{pmatrix} \tag{19}$$

TABLE I
LIST OF PARAMETERS USED IN THE MODEL

| Symbol | Value | Description |
|---|---|---|
| $A$ | $1.0\times10^{8}\,s^{-1}$ | nonradiative recombination constant |
| $B$ | $2.5\times10^{-17}\,m^{3}s^{-1}$ | bimolecular recombination constant |
| $C$ | $9.4\times10^{-41}\,m^{6}s^{-1}$ | Auger recombination constant |
| $a_1$ | $2.5\times10^{-20}\,m^{2}$ | material gain constant |
| $a_2$ | $1.5\times10^{19}\,m^{-3}$ | material gain constant |
| $a_3$ | $2.7\times10^{-32}\,m^{4}$ | material gain constant |
| $R_1$ | $5.0\times10^{-5}$ | input facet reflectivity |
| $R_2$ | $5.0\times10^{-5}$ | output facet reflectivity |
| $\beta$ | $1.0\times10^{-4}$ | spontaneous emission factor |
| $n_0$ | $1.1\times10^{24}\,m^{-3}$ | carrier density at transparency |
| $\eta$ | 60% | carrier injection efficiency |
| $N_{TE0}$ | 4.03 | effective refractive index of active region for TE mode |
| $N_{TM0}$ | 3.95 | effective refractive index of active region for TM mode |
| $\Gamma_{TE}$ | 0.18 | optical confinement factor for TE mode |
| $\Gamma_{TM}$ | 0.12 | optical confinement factor for TM mode |
| $dN_{TE}/dn$ | $-1.44\times10^{-26}\,m^{3}$ | differential refractive index for TE mode |
| $dN_{TM}/dn$ | $-1.20\times10^{-26}\,m^{3}$ | differential refractive index for TM mode |
| $\alpha_1$ | $3000\ m^{-1}$ | effective loss coefficient |
| $\alpha_2$ | $2.7\times10^{-21}\,m^{2}$ | effective loss coefficient |
| $q$ | $1.602\times10^{-19}\,C$ | electron charge |

## III. SIMULATIONS AND EXPERIMENTAL RESULTS

Based on the discussions in Section II, a program was developed to generate the carrier distribution in SOA active region. The carrier-density-dependent refractive index for TE and TM propagation are estimated, and the variations of azimuth and ellipticity angle of the probe light with varying pump-light power are predicted. This section examines some of the basic properties of these simulations. The comparisons with experimental investigations are also demonstrated. Table I displays the value of the parameters used in the simulations. The parameters are mostly taken from Kamelian Ltd. and [16]. Some other values are taken from the literature, since they are widely accepted and can be applied to most SOA structures based on InGaAsP/InP material system.

### A. Nonuniform Distributions of Carrier Density Based on Multisection Model

The SOA in this paper is a commercially available pigtailed SOA (Kamelian, OPA series), employing a tensile-strained bulk InGaAsP/InP active region. The polarization sensitivity is less than 0.42 dB, and the gain ripple is around 0.25 dB. The active layer consists of a rectangle active region and taper regions at each end. For the sake of simple computation, we estimated the mean length of the active region by following the assumption made in [16], which is 920 $\mu$m in the case of Kamelian SOA. This is a rough approximation, but it is evidently an approximation in the real physical scenario within an SOA active region and allows consideration of carrier-density nonuniformity owing to poor mobility.

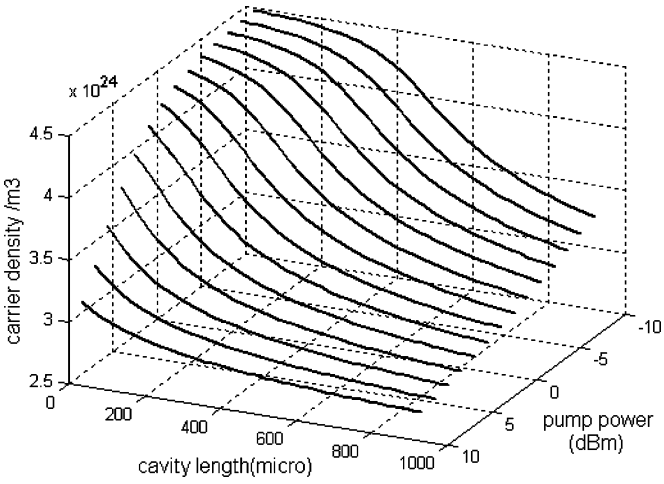


Fig. 3. Simulated carrier density along the SOA cavity at different input pump-light levels.

Fig. 3 shows the computer-generated plots of carrier density along the cavity length with varying pump-light power. This is a 40-section simulation, and the pump power is from $-10$ to 10 dBm. When the pump power is low (e.g., $-8$ dBm), at the SOA input facet, the photon density and stimulated recombination rate are low. Therefore, the carrier-density distributions close to the input facet are most uniform. As the photon density increases along the cavity length, stimulated recombination increases and eventually reaches its maximum. As a result, the carrier density is greatly reduced. For a large pump power (e.g., 8 dBm), the situation becomes simple. Since the photon density is high at the SOA input facet, the stimulated recombination rate is high (the effective carrier lifetime is short), the carrier

density is reduced dramatically near the input facet and reaches a steady state very quickly toward the SOA output facet. These two situations described above are depicted schematically in the three-dimensional (3-D) plot of Fig. 3, together with some intermedial transitions from low to high pump power, showing longitudinal carrier-density distributions. In what follows, we will find that these nonuniform carrier distributions have great impacts on the discrepancy of refractive index between TE and TM propagation and are of practical importance in investigating and modeling the nonlinear polarization rotation of the probe light in a pump–probe scheme.

Before any further analysis, we first address another practical issue: How many sections are needed, or appropriate, for an accurate prediction in a multisection model?

### *B. Number of Sections in a Multisection Model*

A number of models were developed to account for the longitudinal nonuniformity by multisection approach in the past years. Among them, Talli and Adams [28] proposed an eight-section model to simulate the ASE spectrum in SOAs. Durhuus *et al.* [29] treated the TW amplifier as a succession of ten sections, allowing the consideration of the longitudinal nonuniformity. Whereas, Soto and Erasme [30] used a ten-section model to analyze the switching response of SOAs and claimed no significant difference compared with a 50-section model in their modeling.

In order to demonstrate the importance of sectioning number being used in the model and prove our reasoning of choice, phase shift of the probe light as a function of pump-light level is estimated, which serves as a criterion for choosing the number of sections. The simulations are illustrated in Fig. 4. The pump power is from $-8$ to 8 dBm with 0.5-dBm increment, in compliance with our experimental investigations. For a five-section model, as shown in Fig. 4, the variation of phase shift from $-8$ to 8 dBm is 195.3°. As the number of sections increase, the plots move downward and converge to a certain point. The last one in Fig. 4 is a 50-section model and the phase variation is 234.1°.

A more detailed computation reveals that as the number of sections increases, the variations of phase shift increase gradually and eventually converge to 232.2° of a 35-section model and no significant deviations for models with sectioning number larger than 35. This convergence is depicted clearly in the inset of Fig. 4. Thus, for amplifier cavity length of 920 $\mu$m and bias current of 200 mA, 25 sections or more are needed in the numerical modeling to correctly predict the variations of this phase shift. If small sectioning number is used, such as ten sections in Fig. 4, the nonlinear effects are considerably underestimated, leading to an incorrect prediction.

In this modeling work, the maximum sectioning number that has ever been used is 184. The computation time, based on MATLAB 6.0, is less than 6 s, and the phase shift shows little difference from a 40-section model. Therefore, 40 sections are used in the modeling without losing the significance of nonlinear effects or paying too much simulation time.

It is necessary to point out that the decision of how many sections should be used in the modeling work is closely related to the physical parameters of the SOA, such as amplifier cavity length, waveguide structure, bias current, operation temperature, and which nonlinear activities being modeled. The approach presented in Fig. 4 can serve as a general guidance and is easy to extend to other sectioning modeling.

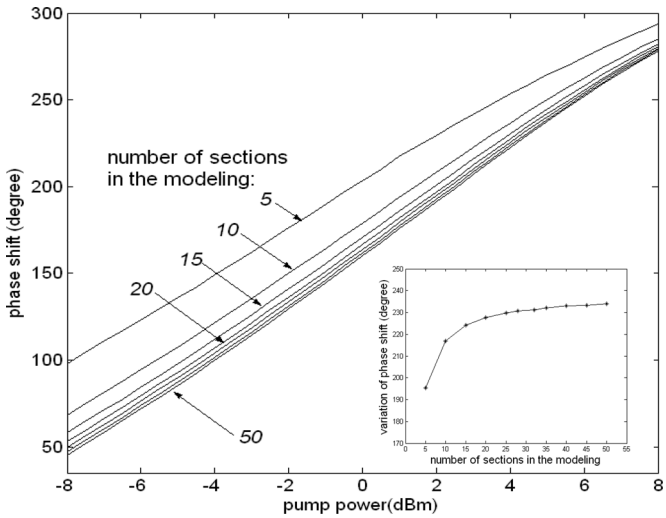


Fig. 4. Simulations of induced phase shift as a function of pump-power level. The numbers next to each plot indicate how many sections are used in the modeling. The inset displays the convergence of phase-shift variations as the sectioning number increases.

### *C. Mueller-Matrix Approach*

Given the Stokes parameters of the incoming probe light, based on (12)–(21), we predict the variations of azimuth and ellipticity angle of the probe light with varying pump power. The trajectories are displayed in Fig. 5 for two different initial Stokes parameters. In Fig. 5(a), the initial value is $S = [1 \quad 0.68 \quad -0.71 \quad 0.03]$. As the pump power increases, the azimuth and ellipticity angle trace out two sine-wavelike trajectories and both cross 0°. As we will demonstrate in Section IV, in a typical pump–probe setup, it is crucial to tune the ellipticity angle close to 0° because it can guarantee the polarizer to find a null position in the similar principle of ellipsometry technology [13]. This crossing-zero position, which is highlighted by a dotted line in Fig. 5(a), is more profound when trying to achieve high extinction ratio in the applications of wavelength conversion [5] and optical logic gate [31]. Unlike ellipticity angle, it is not necessary to make azimuth angle to cross 0° since one can always adjusts the principal axes of the polarizer to match the polarization azimuth of the probe. The situation in Fig. 5(b) is just the opposite, with initial Stokes parameters $S = [1 \ 0.43 \ 0.42 \ -0.80]$ tracing out two cosine-wavelike trajectories. It is worth to note that the ellipticity angle also crosses 0°, indicated by a dotted line, which assumes a better extinction ratio in a pump–probe scheme. In some extreme cases, when the initial Stokes parameters are chosen improperly, although the trajectories still follow a sine or cosine wave, the ellipticity angle does not go to 0°, which leads to a poor extinction ratio and degrades the system performance. It deserves some careful consideration when initializing the incoming probe

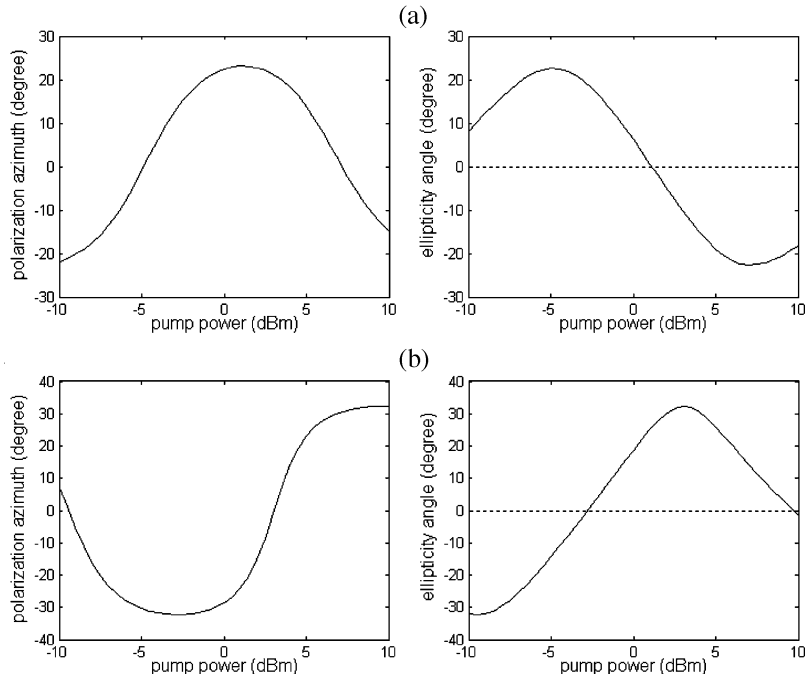


Fig. 5. Simulated trajectories of azimuth and ellipticity angle with varying pump power for two different initial Stokes parameters of the probe light. (a) $S = [1 \;\; 0.68 \;\; -0.71 \;\; -0.03]$. (b) $S = [1 \;\; 0.43 \;\; 0.42 \;\; -0.80]$.

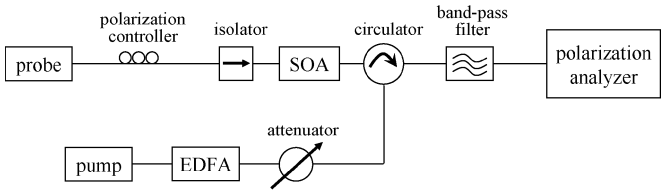


Fig. 6. Experimental setup for the pump and probe geometry in a counter-propagating scheme.

polarization. Fortunately enough, the initial Stokes parameters can be adjusted by a polarization controller, and crossing zero trajectories can somehow always be realized.

### *D. Experimental Investigations*

From an application point of view, the variation of ellipticity angle is more important than that of azimuth angle in a pump–probe scheme since this phase variation can be virtually detected by a linear polarizer and be converted into intensity variation. Therefore, in the following experimental demonstrations, we will focus on the dependence of ellipticity angle on pump-power levels. The experimental setup is shown in Fig. 6. A polarization controller is placed right after the probe light to adjust the SOP of the probe. A bandpass filter (1 nm) is placed before the polarization analyzer to sufficiently suppress the spontaneous noise from the SOA. Throughout the experiment, polarization-maintaining (PM) fibers are used. The power of the probe coupled into the SOA is around $-8$ dBm, and the power of the pump light coupled into the SOA is modified by an attenuator.

Generally, the exact input polarization is difficult to measure, since the SOA has a pigtail of standard single-mode fiber. In practice, the input polarization is adjusted by using a polarization controller before the SOA. Significant changes of ellipticity angle but with different amounts are observed for different input polarizations, indicating input-polarization sensitivity of the pump–probe scheme. This is shown in Fig. 7(a) and (b) for two different initial Stokes parameters: 1) $[1 \;\; 0.73 \;\; -0.46 \;\; 0.13]$ and 2) $[1 \;\; 0.75 \;\; -0.4 \;\; 0.37]$. The increment of pump power is 0.5 dBm in both cases. Solid lines in the plot are theoretical predictions, while asterisks are experimental results.

One of the uncertainties associated with the measurement lies in the insufficient knowledge of pump power coupled into the SOA. During the experiments, we experienced some difficulties in coupling more pump power beyond 7 dBm into the SOA. This is probably due to the limited maximum output power from Santec laser source and erbium-doped fiber amplifier (EDFA) used. Other optical losses include coupling loss and accumulated losses from the components in the experiment. Meanwhile, when the pump power in the cavity is too low, carrier-density depletion is not significant. This situation is shown in Fig. 3 in association with carrier longitudinal distribution. Low-power pump light cannot induce any refractive-index nonlinearity, and the pump–probe scheme lost its significance. Therefore, no experimental observations can be made. This is the case in Fig. 7(a) and (b) when pump light is less than $-7$ dBm. For pump power between $-7$ and 7 dBm, the rolloff of the ellipticity-angle trajectories as predicted by the model are in good agreement with the experiments, which prove the validity of our simulations.

Although the simulation gives a good prediction, shown in Fig. 7(a), there exist some discrepancies between the experiments and simulation results, as shown in Fig. 7(b). These can be attributed to the sensitive nature of polarization rotation in SOAs. The degree of sensitivity in the pump–probe scheme

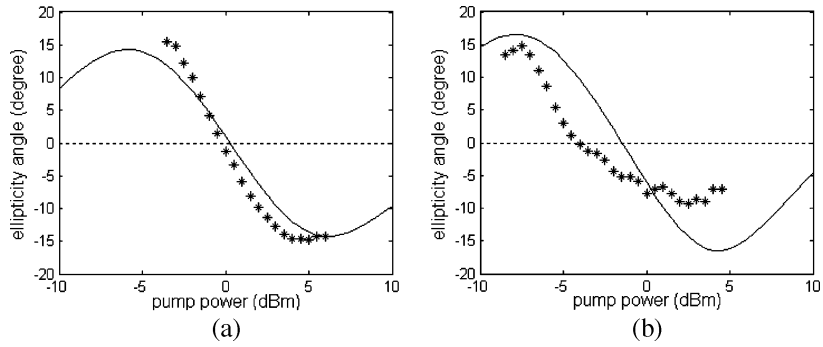


Fig. 7. Ellipticity angle variations as a function of pump light power. Stokes parameters of the incoming probe is (a) $[1 \quad 0.73 \quad -0.46 \quad 0.13]$ and (b) $[1 \quad 0.75 \quad -0.4 \quad 0.37]$. Solid line: Simulation. Asterisk: Experimental result.

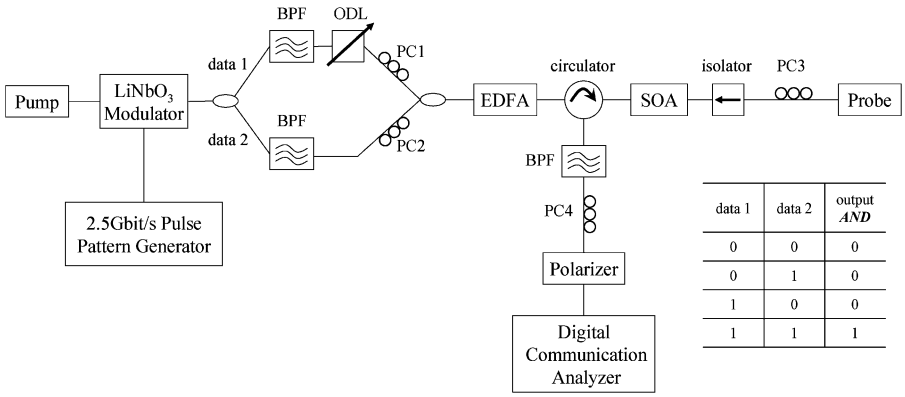


Fig. 8. Experimental setup for optical AND gate with truth table. BPF: bandpass filter. ODL: optical delay line. PC: polarization controller. EDFA: erbium-doped fiber amplifier.

has yet to be fully investigated but will be a subject of future work. Meanwhile, it is interesting to note that the measured SOP is not exactly that of the SOA, e.g., the optical trace demonstrated in [5] in the form of Poincaré sphere. It also contains contributions from the circulator and bandpass filter after the SOA. In practice, it is the overall evolution of the polarization variation that is of practical importance in the applications of all-optical signal processing.

## IV. Applications

Previously, we reported wavelength conversion based on the carrier-induced nonlinearities in SOAs [5]. In this section, we present an optical AND gate operating at a bit rate of 2.5 Gb/s by the same physical principle. The setup is displayed in Fig. 8 along with a truth table.

In this paper, the bias current of Kamelian SOA is 200 mA and operation temperature is maintained at 20 °C. The power of continuous-wave probe signal, at a wavelength of 1555.6 nm, is about −8 dBm at the SOA input. The pump light, at 1545.6 nm, is modulated at a bit rate of 2.5 Gb/s via a $LiNbO_3$ Mach–Zehnder modulator. Data 1 and data 2 are obtained by splitting the pump light into two data trains by a PM splitter. The application of an optical delay line (ODL) in data 1 is to produce "1001" pulse trains, which is different from "0011" trains of data 2 in the other arm. After being combined by a PM combiner, data 1 and data 2 are amplified by an EDFA and are coupled into the SOA by an optical circulator. A 1-nm bandpass filter is placed after the circulator to sufficiently suppress the spontaneous noise from the SOA. Throughout this paper, PM fibers, a PM splitter, and a PM combiner are used. The optical output data is measured on an HP83480A digital communications analyzer with a 20-GHz O/E plug-in module (HP83485A). Fig. 9 presents the operation of optic AND gate.

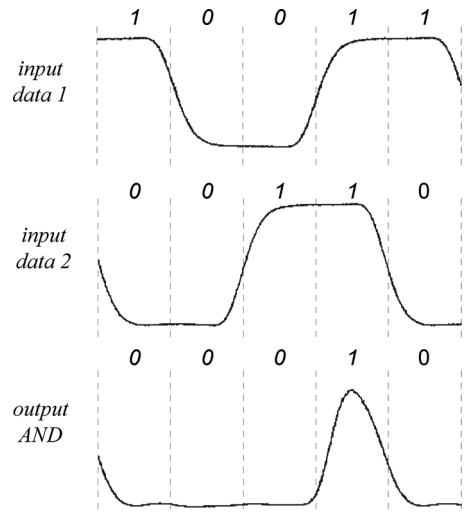


Fig. 9. Optical AND operation.

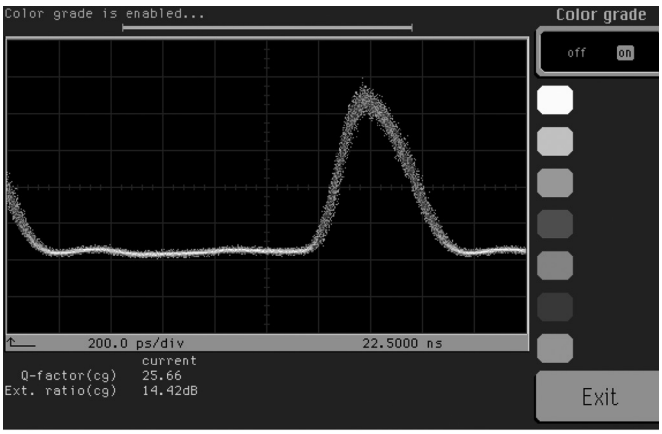


(a)

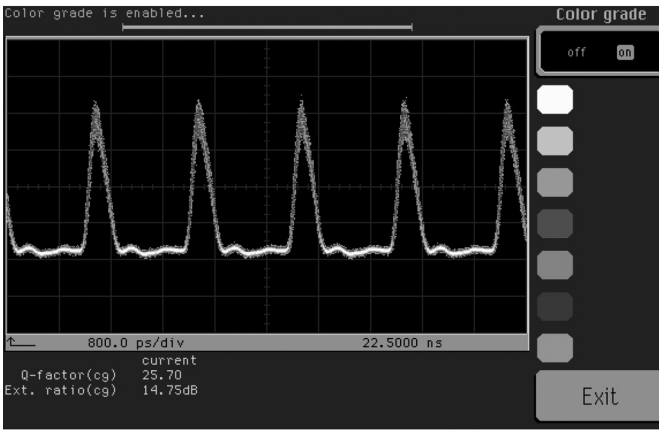


(b)

Fig. 10. Optical traces displayed on the digital communications analyzer with the value of Q-factor and extinction ratio. (a) 200 ps/div. (b) 800 ps/div.

The principles of AND operation can be described as follows: During the logic operation, the absence of both data 1 and data 2 does not change the SOP of the probe. One data alone could not change the SOP dramatically, and the small change cannot be detected by the polarizer before the digital communications analyzer. When both data 1 and 2 are presented inside the SOA, due to high light intensity, the polarization azimuth and ellipticity angle of the probe will be modified, and an optical polarizer can eventually detect the difference and convert the variations of ellipticity angle into intensity variations. Therefore, optical AND gate is realized. Fig. 10 demonstrates the realization of the AND function. The optical traces are directly recorded from the digital communications anaylzer with 1) 200 ps/div and 2) 800 ps/div. The difference between logic "1" state and logic "0" state is $> 160\ \mu$W. This amplitude is large enough to distinguish the two levels. As shown in Fig. 10, high extinction ratio (14.4 dB) with better Q-factor (25.7) is achieved, indicating the superiority of this optical logic gate.

The advantage of this new approach of optical-logic-gating scheme is its immunity against small-signal distortion in the "0" state and a potentially large extinction ratio improvement with high Q-factor. These result from the fact that XGM takes place simultaneously with refractive-index nonlinearity in the SOA. By carefully choosing the operation scheme, the XGM effect can actually enhance the difference between logic "1" state and logic "0" state [5], which leads to a much improved extinction ratio. It should be noted, however, that careful control of input polarization is required in this new scheme due to the pump and probe polarization sensitivity, which may be disadvantageous in some circumstances, but this approach could be extended to more practical applications with some polarization-diversity scheme.

## V. Discussions

### A. Degree of Polarization (DOP)

In this paper, we noted that the DOP of the probe light, either before or after the SOA, is not exactly 100%. Most of the time, it is around 95%. Up to now, no experimental indications are found in published works for a partially polarized light in pump and probe geometry and detailed studies of the ellipticity variations of a partially polarized light in pump–probe scheme have not yet been made.

It has previously been pointed out that only the polarizer and improper rotation matrices do not decrease the DOP for any input Stokes vectors [32]. Therefore, the partially polarized light is most likely from the Santec laser itself. Our concern lies in the treatment of SOP variations by Mueller matrix, which is based on a fully polarized light. However, measurements of ellipticity variations are in good agreement with model predictions in this paper, which gives a reasonable description of the dependence of ellipticity variation with carrier density, at least for probe light with DOP larger than 95%.

### B. Multiple-Quantum-Well (MQW) SOAs

SOAs have been known for decades now to benefit from the use of MQWs. Specific advantages include

1) enhanced differential gain associated with reduced (2-D) density of states;
2) fast gain-recovery time, typically on the order of 10 ps or less [33];
3) enhanced differential refractive index, as much as 1.8 greater than that of conventional bulk structure [34];
4) broad gain bandwidth by well/barrier engineering [35];
5) suppression of Auger recombination achieved via band-structure engineering; and
6) large saturation output power and high characteristic temperature.

Due to the multilayered nature of MQWs, the optical gain in MQWs SOAs is strongly wavelength-dependent [36]. Meanwhile, the effective refractive index is a complicated function of multilayered structure, which can be solved by the so-called "zero-transfer matrix-element method" [37] with the help of "effective-index method" [13].

Inspection of (19) shows that, for MQWs SOAs, the Mueller matrix is also a function of TE and TM gain since $G_{\mathrm{TE}} = G_{\mathrm{TM}}$ is not valid for broad gain spectrum and cannot be abstracted and further eliminated from the expressions of (20) and (21). As a result, the azimuth and ellipticity angles of the transmitted probe light are also TE- and TM-gain-dependent. In comparison with bulk SOAs, this complicates the present

analysis considerably. It is beyond the scope of this paper to go into a detailed discussion of this topic, and the modeling of employing MQWs SOAs as a nonlinear medium in pump and probe geometry can be considered a matter of ongoing research.

## VI. Summary

Multisection steady-state solutions of the rate equations for a TW-type tensile-strained bulk SOA are presented in this paper. The significant nonuniform carrier density across the active region is demonstrated from sectioning calculations of the carrier and photon densities as a function of pump-power levels. This numerical approach is more appropriate than generalized analytic equations for predicting nonuniform distributions of carrier density in amplifier cavity.

We have investigated the carrier-density-dependent refractive indexes for TE and TM propagation. The existing differences on carrier density nonuniformity lead to the variations of azimuth and ellipticity angle of a probe under varying pump power. The variations are predicted by Mueller-matrix formalism, which greatly simplifies the variation analyses. Good agreement between theoretical and experimental results on the variations of ellipticity angle is obtained in the presence of intense pump light, supporting the validity of the model. An optical AND gate is realized based on this nonlinear mechanism in SOAs. Although the model in this paper is developed for bulk SOAs by following the discussion we made in Section V-B, it can be extended to MQWs SOAs, with some modifications in (19)–(21) to take into account the multilayered waveguide structure.

In comparison with the Jones matrix, the Mueller-matrix approach shows a lot of advantages in terms of simplicity and accuracy. Perhaps the biggest benefit lies in the fact that during the optical-tuning process, Stokes parameters of the probe can be monitored by a polarization analyzer and readily compared with numerical modeling. While the problems could be treated using the amplitude formulation, the use of the Mueller-matrix formalism greatly simplifies the simulation herein.

## Acknowledgment

L. Q. Guo would like to thank Dr. Z. Peng and Dr. D. Tong of McMaster University, Hamilton, ON, Canada, for their technical advice and stimulating discussions.

## References

[1] M. J. Connelly, *Semiconductor Optical Amplifiers*. Boston, MA: Kluwer, 2002.

[2] D. Cotter, R. J. Manning, K. J. Blow, A. D. Ellis, A. E. Kelly, D. Nesset, I. D. Phillips, A. J. Poustie, and D. C. Rogers, "Nonlinear optics for high-speed digital information processing," *Science*, vol. 286, no. 5444, pp. 1523–1528, Nov. 1999.

[3] J. Mork, A. Mecozzi, and G. Eisenstein, "The modulation response of a semiconductor laser amplifier," *IEEE J. Sel. Topics Quantum Electron.*, vol. 5, no. 3, pp. 851–860, May/Jun. 1999.

[4] M. F. C. Stephens, M. Asghari, R. V. Penty, and I. H. White, "Demonstration of ultrafast all-optical wavelength conversion utilizing birefringence in semiconductor optical amplifiers," *IEEE Photon. Technol. Lett.*, vol. 9, no. 4, pp. 449–451, Apr. 1997.

[5] L. G. Guo and M. J. Connelly, "Signal-induced birefringence and dichroism in a tensile-strained bulk semiconductor optical amplifier and its application to wavelength conversion," *J. Lightw. Technol.*, vol. 23, no. 12, pp. 4037–4045, Dec. 2005.

[6] H. J. S. Dorren, D. Lenstra, Y. Liu, M. T. Hill, and G.-D. Khoe, "Nonlinear polarization rotation in semiconductor optical amplifiers: Theory and application to all-optical flip-flop memories," *IEEE J. Quantum Electron.*, vol. 39, no. 1, pp. 141–148, Jan. 2003.

[7] J. P. Turkiewicz, G. D. Khoe, and H. de Waardt, "All-optical 1310 to 1550 nm wavelength conversion by utilizing nonlinear polarization rotation in semiconductor optical amplifier," *Electron. Lett.*, vol. 41, no. 1, pp. 29–30, Jan. 2005.

[8] H. Soto, J. D. Topomondzob, D. Erasmeb, and M. Castro, "All-optical NOR gates with two and three input logic signals based on cross-polarization modulation in a semiconductor optical amplifier," *Opt. Commun.*, vol. 218, no. 4–6, pp. 243–247, Apr. 2003.

[9] E. Alvarez, H. Soto, and J. Torres, "Investigation of the carrier density dependence on the confinement factor in a bulk semiconductor optical amplifier with a ridge waveguide," *Opt. Commun.*, vol. 222, no. 1–6, pp. 161–167, Jul. 2003.

[10] M. Zhao, J. D. Merlier, G. Morthier, and R. Baets, "Dynamic birefringence of the linear optical amplifier and application in optical regeneration," *IEEE J. Sel. Topics Quantum Electron.*, vol. 8, no. 6, pp. 1399–1404, Nov./Dec. 2002.

[11] H. Soto, D. Erasme, and G. Guekos, "Cross-polarization modulation in semiconductor optical amplifiers," *IEEE Photon. Technol. Lett.*, vol. 11, no. 8, pp. 970–972, Aug. 1999.

[12] N. Pfeffer, F. Charra, and J. M. Nunzi, "Phase and frequency resolution of picosecond optical Kerr nonlinearities," *Opt. Lett.*, vol. 16, no. 24, pp. 1987–1989, Dec. 1991.

[13] L. Q. Guo, "Broad-band antireflection coatings for improved grating-external-cavity diode laser performance," Ph.D. dissertation, Dept. Eng. Physics, McMaster Univ., Hamilton, ON, Canada, 2002.

[14] J. Wang, H. Olesen, and K. E. Stubkjaer, "Recombination, gain and bandwidth characteristics of 1.3-$\mu$m semiconductor laser amplifiers," *J. Lightw. Technol.*, vol. LT-5, no. 1, pp. 184–189, Jan. 1987.

[15] G. P. Agrawal and N. K. Dutta, *Semiconductor Lasers*, 2nd ed. New York: Van Nostrand Reinhold, 1993, ch. 11.

[16] M. J. Connelly, "Wideband semiconductor optical amplifier steady-state numerical model," *IEEE J. Quantum Electron.*, vol. 37, no. 3, pp. 439–447, Mar. 2001.

[17] M. Asada, A. R. Adams, K. E. Stubkjaer, Y. Suematsu, Y. Itaya, and S. Arai, "The temperature dependence of the threshold current of GaInAsP/InP DH lasers," *IEEE J. Quantum Electron.*, vol. QE-17, no. 5, pp. 611–619, May 1981.

[18] H. Kawaguchi, *Bistabilities and Nonlinearities in Laser Diodes*. Boston, MA: Artech House, 1994, ch. 4.

[19] R. Olshansky, C. B. Su, J. Manning, and W. Powazinik, "Measurement of radiative and nonradiative recombination rates in InGaAsP and AIGaAs light sources," *IEEE J. Quantum Electron.*, vol. QE-20, no. 8, pp. 838–854, Aug. 1984.

[20] M. Kot and K. Zdansky, "Measurement of radiative and nonradiative recombination rate in InGaAsP-InP LED's," *IEEE J. Quantum Electron.*, vol. 28, no. 8, pp. 1746–1750, Aug. 1992.

[21] L. A. Coldren and S. W. Corzine, *Diode Lasers and Photonic Integrated Circuits*. New York: Wiley, 1995, ch. 4.

[22] ——, *Diode Lasers and Photonic Integrated Circuits*. New York: Wiley, 1995, App. 4.

[23] E. Wintner and E. P. Ippen, "Nonlinear carrier dynamics in GaInAsP compounds," *Appl. Phys. Lett.*, vol. 44, no. 10, pp. 999–1001, May 1984.

[24] D. T. Cassidy, "Spontaneous-emission factor of semiconductor diode lasers," *J. Opt. Soc. Amer. B, Opt. Phys.*, vol. 8, no. 4, pp. 747–752, Apr. 1991.

[25] K. L. Hall, E. R. Thoen, and E. P. Ippen, "Nonlinearities in active media," in *Semiconductors and Semimetals*, vol. 59. San Diego, CA: Academic, 1999, p. 83.

[26] L. Q. Guo and M. J. Connelly, "Demonstration of birefringence in a bulk semiconductor optical amplifier and its application to all-optical wavelength conversion," in *Proc. Symp. Opt. Fiber Meas.*, P. A. Williams and G. W. Day, Eds., 2004, pp. 167–170.

[27] D. Goldstein, *Polarized Light*, 2nd ed. New York: Marcel Dekker, 2003, ch. 6.

[28] G. Talli and M. J. Adams, "Amplified spontaneous emission in semiconductor optical amplifiers: Modeling and experiments," *Opt. Commun.*, vol. 218, no. 1–3, pp. 161–166, Mar. 2003.

[29] T. Durhuus, B. Mikkelsen, and K. E. Stubkjaer, "Detailed dynamic model for semiconductor optical amplifiers and their crosstalk and

intermodulation distortion," *J. Lightw. Technol.*, vol. 10, no. 8, pp. 1056–1065, Aug. 1992.

[30] H. Soto and D. Erasme, "Modeling and experimental measurements of the switching behavior of semiconductor optical amplifiers," *Opt. Quantum Electron.*, vol. 28, no. 6, pp. 669–682, Jun. 1996.

[31] L. Q. Guo and M. J. Connelly, "All-optical AND gate using nonlinear polarization rotation in a bulk semiconductor optical amplifier," in *Proc. Tech. Dig.: Opt. Amplif. and Their Appl.*, Washington, DC: Opt. Soc. Amer., 2005, pp. 1–3. Pres. no.: SuB9.

[32] S. Y. Lu and R. A. Chipman, "Mueller matrices and the degree of polarization," *Opt. Commun.*, vol. 146, no. 1–6, pp. 11–14, Jan. 1998.

[33] J. M. Wiesenfeld, A. H. Gnauck, G. Raybon, and U. Koren, "High-speed multiple-quantum-well optical power amplifier," *IEEE Photon. Technol. Lett.*, vol. 4, no. 7, pp. 708–711, Jul. 1992.

[34] J. Jacquet, P. Brosson, A. Olivier, A. Perales, A. Bodere, and D. Leclerc, "Carrier-induced differential refractive index in GaInAsP-GaInAs separate confinement multiquantum well lasers," *IEEE Photon. Technol. Lett.*, vol. 2, no. 9, pp. 620–622, Sep. 1990.

[35] M. J. Hamp, "Asymmetry multiple quantum well lasers," Ph.D. dissertation, Dept. Eng. Physics, McMaster Univ., Hamilton, ON, Canada, 2000.

[36] R. W. H. Engelmann, C.-L. Shieh, and C. Shu, "Multiquantum well lasers: Threshold considerations," in *Quantum Well Lasers*, P. S. Zory, Ed. New York: Academic, 1993.

[37] L. M. Walpita, "Solutions for planar optical waveguide equations by selecting zero elements in a characteristic matrix," *J. Opt. Soc. Amer. A, Opt. Image Sci.*, vol. 2, no. 4, pp. 595–602, Apr. 1985.

**L. Q. Guo**, photograph and biography not available at the time of publication.

**Michael J. Connelly** (S'89–M'92) was born in Limerick, Ireland, in 1965. He received the B.E. and Ph.D. degrees in electronic engineering from the National University of Ireland, Dublin, in 1987 and 1992, respectively.

He is a Senior Lecturer in electronic engineering and Director of the Optical Communications Research Group at the University of Limerick. His current research interests include semiconductor-optical-amplifiers (SOAs), static and dynamic modeling, all-optical signal processing using SOAs, optical coherence tomography, and laser vibrometry.